THESIS

GAS TURBINE COMMISSIONING AND INTAKE DESIGN FOR UTILIZATION OF EXHAUST GAS RECIRCULATION USING COMPUTATIONAL FLUID DYNAMICS

Submitted by

Andrew Harrod

Department of Mechanical Engineering

In partial fulfillment of the requirements
For the Degree of Master of Science
Colorado State University
Fort Collins, Colorado
Fall 2025

Master's Committee:

Advisor: Bret Windom

Daniel Olsen
Jeremy Daily

ABSTRACT

GAS TURBINE COMMISSIONING AND INTAKE DESIGN FOR UTILIZATION OF EXHAUST GAS RECIRCULATION USING COMPUTATIONAL FLUID DYNAMICS

As Earth's climate changes at a rapid pace, the power generation industry is exploring ways to reduce carbon emissions without significantly affecting the operation of the existing gas turbine fleet which accounts for a large amount of the industry's output. This research investigates the reduction of carbon emissions from a 3.5 MWe Solar Turbines Centaur 40 power generation gas turbine by implementing exhaust gas recirculation (EGR) in conjunction with carbon capture technologies. This thesis focuses on integrating recirculated exhaust into the gas turbine's air intake system, with emphasis on the design of the exhaust gas recirculation (EGR) mixer and the commissioning of supporting sub-systems for a future experimental setup. This work is split into two sections: EGR mixer design using numerical analysis and commissioning gas turbine experimental test skid.

An EGR mixer will ensure minimal flow distortions and even distribution of exhaust gas at the compressor inlet. The EGR mixer design began with research into similar applications but ultimately resulted in the design of a non-intrusive injection method. Three EGR inlet methods were tested to determine how injection geometry impacts mixing and distorts inlet guide van (IGV) flow. An EGR inlet size sweep was conducted to determine the optimal geometry. The models were then tested using Computational Fluid Dynamics (CFD) simulations, where mixing effectiveness was evaluated and quantified using the Coefficient of Variance (COV), along with pressure and mass flow distortion metrics. Results were measured at the package inlet as well as the IGV plane. It was found that method of injection does affect mixing effectiveness, with

increased injection pressure resulting in better mixing. A wide injection method, spanning an entire duct length, provides the best tradeoff for minimizing flow distortions while maintaining a well-mixed flow.

As regards to the commissioning activities, the intake ducting was designed to meet specifications from Solar Turbines while conforming to lab restrictions within the Colorado State University Energy Campus. Future EGR implementation also had to be considered. Structural integrity assessments and intake duct pressure drop calculations were conducted to verify compliance with manufacturer specifications. A custom filter box and angled duct sections were designed to fit the building structure and accommodate the constraints of the lab space. Enclosure ventilation, purge and drain systems were also designed to meet Solar Turbines specifications, while still conforming to our lab space. Design decisions and hardware specifications of these subsystems are described in this thesis.

ACKNOWLEDGEMENTS

This work was funded by Decarbonization Research Consortium by the Office of Naval Research; awarded as part of grant N00014-23-S-B001. Technical support was provided by Solar Turbines. Lab space, facilities and equipment are graciously provided by the CSU Energy Institute at the Powerhouse Energy Campus.

Many thanks to Dr. Bret Windom who sponsored me throughout this project and provided countless hours of technical advising. Andrew Zdanowicz, a key member to the construction aspects of this project as well as providing invaluable advice. Dr. Toluwalase Fosudo, who continuously motivated me to perform at my highest level.

I have extreme gratitude for the engines lab team: Kirk Evans, Mark James and Erin Kelly. I would not be the engineer I am today without the initial training I had from you.

Bianca Jeremiah and Kinglsey Atomboh, the two students I had the pleasure of researching with for the past two years. I'm grateful for the many laughs and problem-solving sessions.

DEDICATION

To my brother, Brian, and my parents, Jane and Garry. Whose endless support, love and encouragement led through my education.

TABLE OF CONTENTS

LIST OF FIGURES

LIST OF TABLES

Chapter 1-Introduction

1.1 Motivation

High carbon dioxide emissions are expediting global warming. Increasing emission restrictions have called for developments in the energy industry to reduce carbon footprints without changing current infrastructure or ability. Gas turbine engines are commonly powered by natural gas and, in many cases, liquid (diesel) fuel, to produce mechanical work, generate electricity and provide propulsion. While these systems are efficient and widely used in power generation, they rely heavily on fossil fuels, contributing to large greenhouse gas emissions. Natural gas, the most common gas turbine fuel, was responsible for the production of 735.5 million metric tons of CO_2 in 2024 alone [1]. This large release of CO_2 heavily contributes to the current climate crisis. Figure 1 depicts the trend of natural gas and crude oil usage in the production of US energy. Current trends show that dependence on these fuels is rapidly increasing, outpacing all other energy sources.

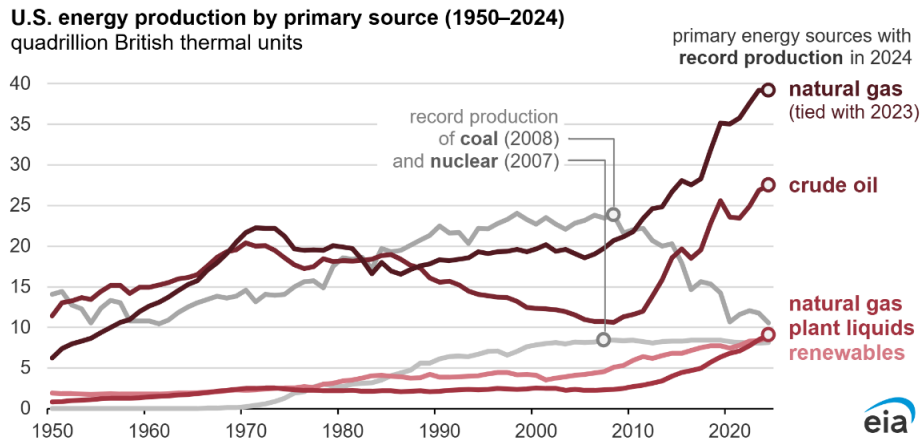

Figure 1: U.S. Energy Production with Primary Source (1950-2024). Comparison of Energy Produced for Natural Gas, Crude Oil, Coal, Nuclear, Natural Gas Plant Liquids and Renewables. Record Production years are labeled. [2]

While the electric grid is increasingly being powered by renewable energy sources, these engines are commonly found in remote and inaccessible locations, such as ships, and cannot be replaced with conventional renewable sources. This requires a different solution to lower their carbon emissions. The Office of Naval Research, a key sponsor of this project, is considering adding carbon capture systems to U.S. Navy ships that are equipped with gas turbines, as a method of reducing global greenhouse gases as seen in Figure 2. Not only will this prevent excess carbon from entering the atmosphere, but the Navy can also repurpose it for fuel synthesis on or offshore. In offshore applications the captured carbon can provide the Navy with a maritime tactical advantage when used for synthesis on nuclear powered vessels by refueling vessels while out at sea.

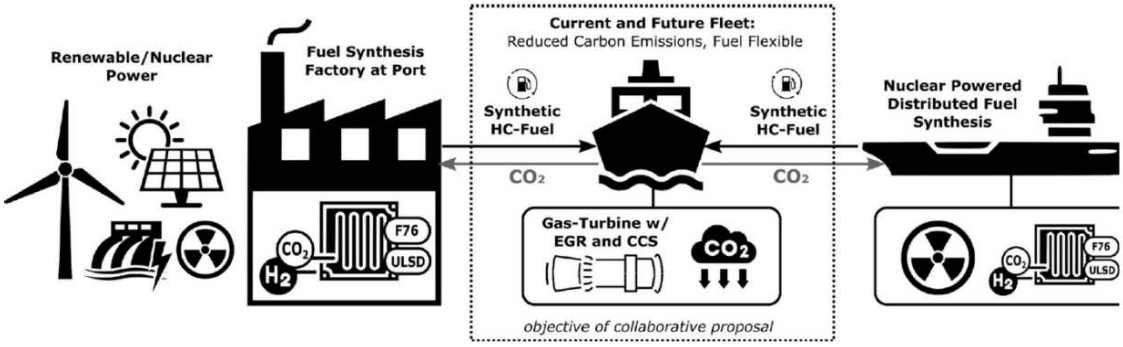

Figure 2: The United States Navy Practical Use Diagram for Use Of Captured Carbon.

1.2 EGR for Gas Turbines

The current research proposes testing an exhaust gas recirculation (EGR) system coupled with a carbon capture system (CCS) as seen in the flow schematic depicted in Figure 3. EGR is the process of redirecting a set portion of the exhaust back into the compressor inlet. The exhaust gas is cooled via a heat exchanger to match the ambient airflow as well as meet CCS requirements. A diverter allows for a variable percentage of exhaust to be recirculated. An inlet

mixer mixes the exhaust gas with the ambient air. A CCS reduces the overall carbon emissions by removing carbon dioxide from the exhaust.

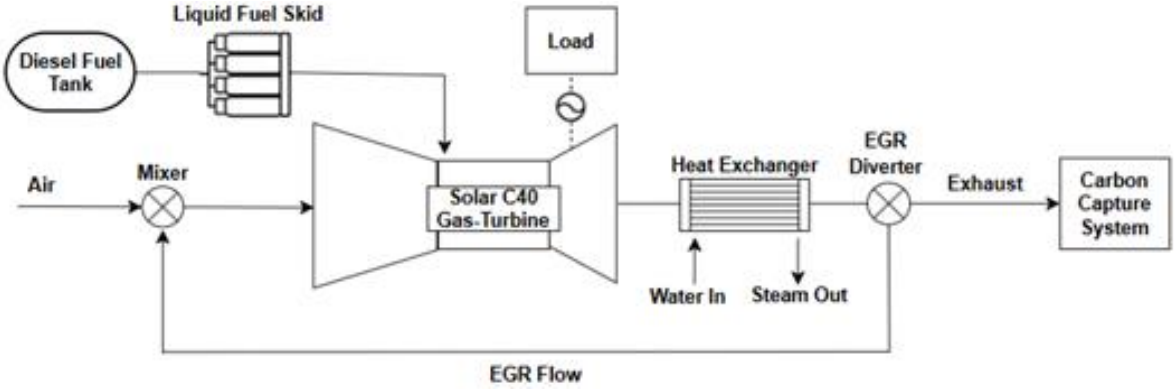

Figure 3: EGR Flow Schematic for Liquid-Fueled Centaur 40 Gas Turbine With CCS.

Gas turbines inherently produce a low concentration of CO_2 in their exhaust, making the installation of a carbon capture system (CCS) impractical due to the large system size required. An EGR system will increase the carbon content in the exhaust system [3] thus enhancing carbon capture efficiency [4]. An increase in CCS efficiency leads to a reduction in system size, enabling deployment on ships and other platforms with limited available space. The size of the CCS decreases as the EGR percentage increases, as shown in Figure 4. Specifically, at 50% EGR, the CCS reduces in size by nearly 30%. A gas turbine EGR system will effectively increase the efficiency of a CCS without majorly disrupting the industry, but it does have impacts on gas turbine performance that need to be investigated.

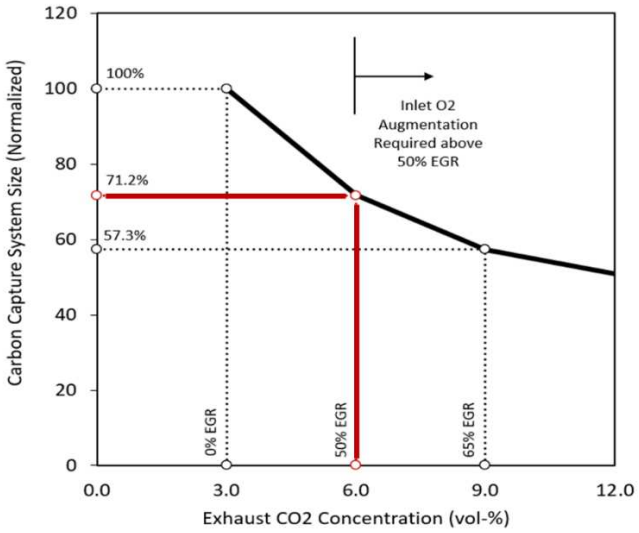

Figure 4: Carbon Capture Size versus Exhaust CO_2 Concentration. Red Lines Highlight the Combustion Limit Where Inlet O_2 Augmentation is Required.

1.3 Effect of EGR on gas turbines

EGR aids CCS by increasing CO_2 in the exhaust, but the displacement of air subsequently impacts combustion and engine operation while also potentially impacting compressor performance. Considerations need to be taken to ensure stable turbine operation is maintained. Understanding these implications is essential before implementing EGR in gas turbines, particularly for retrofitting existing engines.

1.3.1 Combustion Performance

$$C_xH_y + O_2 + N_2 \rightarrow CO_2 + H_2O + N_2 \quad (1)$$

Equation 1 above shows a basic stoichiometric combustion reaction for a hydrocarbon fueled engine without added EGR. Variables X and Y are subject to change for varying fuels. The diesel fuel, a commonly used hydrocarbon fuel in gas turbines, is represented as C_xH_y while the intake air is modeled as a combination of the elements O_2 and N_2. CO_2, N_2, and H_2O are the

products of the reaction if 1 mole of the fuel is assumed to be completely burned in an ideal stoichiometric combustion scenario. Some gas turbines are equipped with a lean burn combustion system for emissions regulations. In a lean burn, there is excess oxygen in the combustion reactants. The premise of EGR is adding the products of the combustion reaction back into the reactants. The engine being researched in this project utilizes a lean burn combustor where the main recirculated products are CO_2, N_2, and O_2.

Oxygen is a required combustion component and will be displaced by the now oxygen-deficient exhaust gases being recirculated. Figure 5 shows that EGR percentages above 50% will require supplemental oxygen and the associated complexities to maintain stable combustion [3]. For this reason, this project scope will investigate EGR at and below 50% to maintain as simple a set-up as possible while harnessing the benefits of the recirculated exhaust gases on combustion and the targeted CO_2 concentrations.

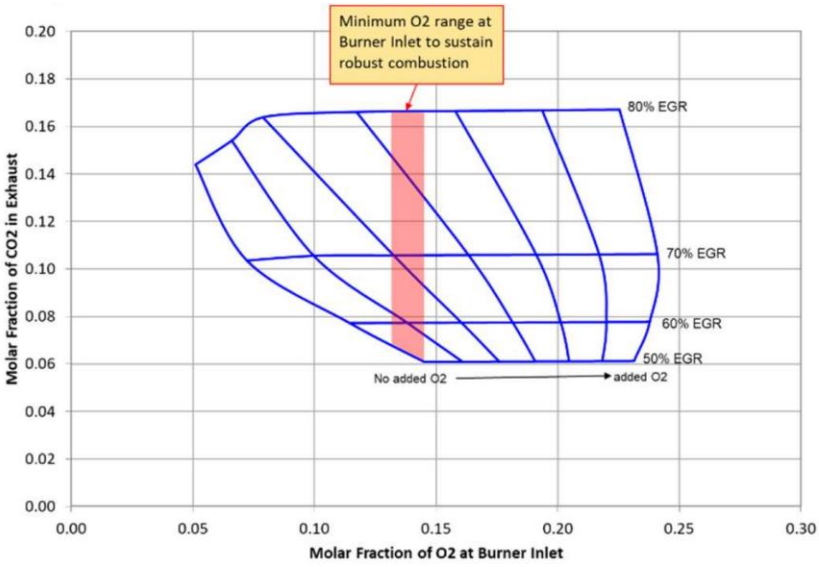

Figure 5: Mole Fraction of O_2 at Burner Inlet vs Mole Fraction of CO_2 in Exhaust with EGR Ranges. Red Band Shows the Region of Stable Combustion [3].

1.3.2 Compressor Performance

Axial compressors utilize a ring of airfoils that compress air in an annular inlet. This compressor inlet is commonly referred as the inlet guide vane (IGV) plane. Compressor IGV (inlet guide vanes) ingestion requirements are designed around the compressor performance limitations, and minimal flow variation among the compressor blades. Which is necessary to maintain compressor performance and avoid flow instabilities [5]. Circumferential flow distortions of density, pressure, and velocity can cause compressor stalls depending on severity. This issue can progress to a rotating stall, a phenomenon where a stall cell rotates with the rotors, at a slower speed, causing extreme stress and vibrations [6]. Alternatively, large flow variations in the axial direction – specifically mass flow and velocity – will result in compressor surge, a phenomenon in which flow reverses in the compressor, causing large pressure variations and damaging vibrations [7]. These vibrations can cause cracking and warping—also known as high cycle fatigue—within the IGVs, which may lead to blade detachment and result in catastrophic failure [8]. The introduction of exhaust gases will affect the density, velocity, and mass flow of the system, increasing the likelihood of stall, surge and high cycle fatigue. Non-optimized inlet duct geometry can cause asymmetric flows and swirl into the IGVs [8]. The recirculated exhaust will be introduced into the intake duct through an EGR mixer as a means of minimizing flow distortions to reduce impacts on compressor performance, the primary focus of the current study.

1.4 Necessity and Role of Mixing in EGR for Gas Turbines

As exemplified in section 1.3 Gas Turbines can be fragile when inlet properties are altered. The scope of this project ends at maintaining the operation and health of the compressor. For more detailed information on compressor and combustion performance implications, please refer to Burnes [3].The sole function of the EGR mixer is to ensure that the recirculated exhaust gas is

adequately mixed with the intake air stream and that flow distortions are minimized. This will ensure that the intake composition will be consistent for all tests, resulting in no adverse compressor performance or health effects. As well as creating a consistent intake stream for repeatable and accurate experimental results.

1.5 Previous Studies and Solutions For Intake EGR Mixing

Devi et al. performed a simulation study on the introduction of EGR into the filter box. The study investigates how a simple square duct plumbed into the filter box will distort the flow at the IGV plane. Devi et al. also performed a study on the placement of flow splitters at the EGR inlet as a method of directing flow and distributing exhaust gas (EG) across the inlet duct. They determined that "pressure and swirl distortions remained almost unaffected with exhaust gas introduction". This research shows that a simple mixing solution with little retrofit modification is feasible. This method also directs exhaust gas through the filters, a potential problem considering backpressure or filter life reduction. Our experimental setup has space restrictions that does not allow for a EGR injection method like this.

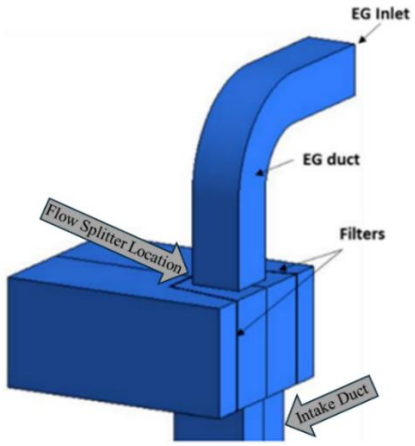

Figure 6: EGR Introduction Method Design Study Performed by Devi et al [9]. Exhaust Gas (EG) is Introduced By a 90 Degree Bend Into The Filter Housing. Mixing Fins are Positioned at the EG and Filter Box Inlet as a Method to Distribute Exhaust Gas.

Lockyer et al. recently published a patent (Figure 7) for an EGR mixer where exhaust gas enters the side of the mixer perpendicular to the ambient air intake below the filters [10]. The exhaust gas enters a mixer which evenly distributes the gas across a grid using a uniform grid of holes across the duct. After speaking with the authors of this patent, they established that their goal was to create an identical inlet flow profile to a gas turbine without an EGR system to negate performance impacts. While this mixer claims to be valid, no public background study has been performed to support its design. A more detailed investigation is needed to explore simpler, more cost-effective solutions that are easier to implement prior to relying on this patented design.

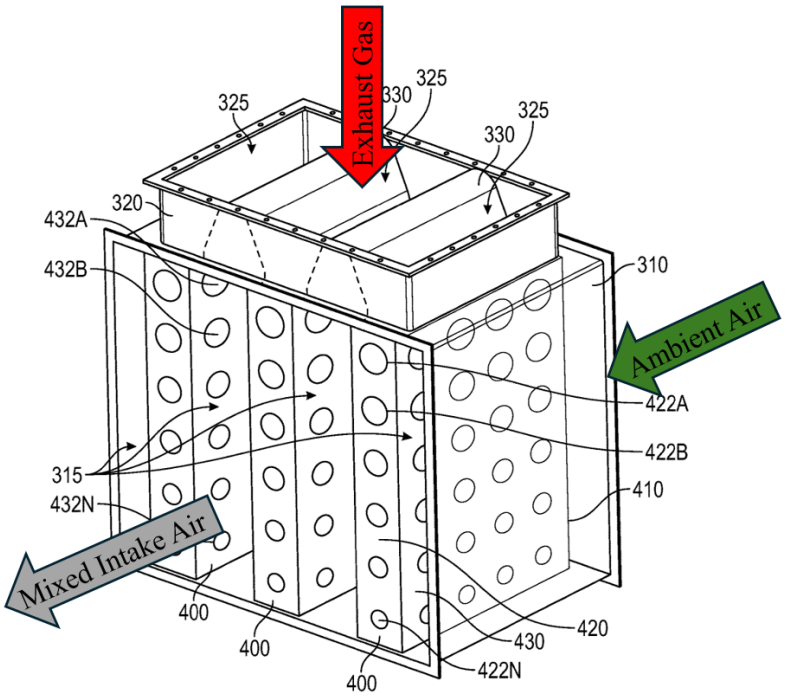

Figure 7: Exhaust Gas Recirculation Mixer Patent by Lockyer et al. [10] Exhaust gas Enters Perpendicular to Ambient Air Flow Through A Uniform of Grid of Holes

1.6 Mixer Distortion Quantification

In their numerical study, Devi et al. investigated the flow characteristics of the mixer using total pressure (PT), total temperature (TT), and swirl distortion (SD) measurements. Distortion was measured using total pressure distortion (PTD) and total temperature distortion (TTD) in equations 2 and 3 [9]. Values are normalized by dividing the local cell value by the averaged IGV plane value. These contours provide a visual distortion plot to highlight abnormalities in the flow. Devi et al. calculated their design total pressure distortion (DPTD) and design total temperature distortion (DTTD) using equations 4 and 5 below. Equations 4 and 5 are only applicable to turbine manufactures because typically a distortion limit is proprietary knowledge.

$$PTD = Total\ Pressure_{local}/Total\ Pressure_{IGV} \tag{2}$$

$$TTD = Total\ Temperature_{local}/Total\ Temperature_{IGV} \tag{3}$$

$$DPTD = (PT_{max@sector} - PT_{\min @\ sector})/(PT_{IGV} * DPTD_{limit}) \tag{4}$$

$$DTTD = (TT_{max@sector} - TT_{\min @\ sector})/(TT_{IGV} * DTTD_{limit}) \tag{5}$$

Solar Turbines specifies a mass flow variation of less than +/-5% across the center line of the intake plane upstream of the compressor annulus [11]. This value is derived from the assumption that flow will evenly wrap around the bulkhead and into the IGV plane. This method of quantification does not provide a foundation for future IGV flow distortion experimental testing. Due to the proprietary nature of OEM published studies, no work was found that openly provides an inlet distortion value.

1.7 Research Question and Objectives

As a method of reducing gas turbine carbon emissions, retrofitting the current gas turbine fleet with an EGR and CCS is being investigated. There have been several studies that validate the justification for an EGR-CCS coupled system, providing adequate motivation. The injection of EGR into a gas turbine can distort intake flow and requires special consideration to maintain normal operation. As described earlier, Devi et al. studied how EGR injected into the filter box distorts flow and provided several methods how to quantify performance. Lockyer et al. published a patent that introduces EGR perpendicular to the intake duct, but public design validation is not provided. Due to restrictions in our experimental setup, a perpendicular injection method is required. Devi et al. only studied EGR introduction upstream of the filters, and Lockyer et al. does not provide justification for their complex design. Taking inspiration from these authors, this research aims to fill in the gaps and contribute more public knowledge on the effect of EGR introduction into a gas turbine intake. The specific goals of this work are as follows:

- Development of a modeling and mixing quantification approach for gas turbine EGR mixers.
- Determine how EGR injection geometries and size contribute to mixing effectiveness and flow distortion at the IGV plane.
- Conduct a fundamental study to understand the tradeoffs between complexity, pressure drop and mixing effectiveness.
- Propose final design and manufacturing plan for an EGR mixer derived from simulation results.

- Design and commissioning of a custom intake system to enable future testing of a Solar Turbines Centaur 40 at the CSU Powerhouse campus with EGR blends.

Injection methods will be tested using Converge CFD, with the objective of identifying a minimally invasive mixer that generates minimal flow distortion at the IGV inlet, while conforming to all OEM and laboratory constraints. A liquid fueled diesel gas turbine will be the sole focus due to sponsor scope, however the following research can be applied to all gas turbine applications from power generation to propulsion.

Chapter 2: Methods

2.1 Experimental Setup

This work is structed around the Solar Turbines Centaur 40 3.515 MWe gas turbine (**Error! Reference source not found.**) currently in the commissioning phase. The Centaur 4 0 intake flow rate is 18.7 kg/s while fuel flow is approximately 0.29 kg/s at full speed and full load. Heat rate is 12,910 kJ/kWe-hr [12]. This engine is used solely for research purposes and is not connected to the university's energy grid, granting the opportunity to perform experiments without operational limitations. SoLoNOx lean burn, dual fuel injectors allow for both liquid and gaseous fuel testing. A 5 gas analyzer and FTIR are available for emission analyzing. Simulation parameters are based off the operating conditions and geometry configurations of the current installation.

Figure 8: Solar Turbines Centaur 40 Gas Turbine Located in CSU Powerhouse Research Campus.

2.2 Mixing Geometry Configurations

To maximize mixing performance of the intake air and the recirculated exhaust gases, several mixer designs were developed and assessed using Converge Computational Fluid Dynamics (CFD) simulations. Figure 8 is a representation of the existing intake duct, with differing injection geometries added, shown in red. The components from top to bottom include the angled section, straight section, intake silencer, and transition duct. Filters were excluded because they do not impact flow direction or velocity magnitude [9]. In reality, the intake silencer is composed of a matrix of cylindrical passages with sound deadening material on the passage walls. To reduce the complexity of the model, the intake silencer geometry was simplified to be a matrix of smooth cylindrical passages as depicted in Figure 9. The silencer acts a flow straightener, inhibiting mixer performance.

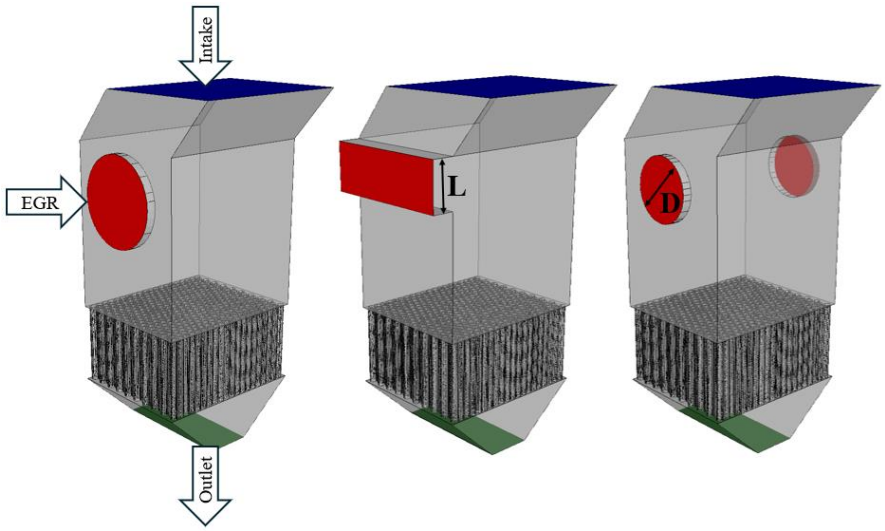

Figure 9: EGR Mixer CFD Simulation Geometries (Left to Right) Control, Wide Injection (WI), Opposed Injection (OI)

Three different EGR mixing geometries were selected for the simulations. A control simulation, featuring a single pipe junction of the same profile as the exhaust, a pipe with a flow

area of 0.82 meters squared. The second profile was a rectangular injection port (WI), stretching the entire length of the duct 1.5 meters. The third profile was two opposed injection (OI) ports. A NO-EGR case was also ran to compare flow distortions caused by EGR injection. A geometry parameter sweep was conducted to optimize the size of these injection ports by adjusting variables length (L) and diameter (D) as pictured in Figure 9. The sweep was performed between the ratio ranges of 2 times and 0.5 times compared to the control size. Mixer performance increases with disturbances in flow, which is often associated with high pressure drops. High pressure drops are a symptom of decreased flow area. Solar Turbines specifies a maximum exhaust pressure loss of 10 inH2O [2.48 kPa] to ensure proper performance. For this reason, the simulations in this work conduct analyses on the tradeoff between mixer effectiveness and the backpressure it exerts on the exhaust stream. Mixing performance results was compared to find optimal geometry shape and size. Mixer performance was quantified at the inlet duct outlet plane, illustrated in green in Figure 9.

To validate impact on compressor performance, the best performing cases were then simulated though the intake bulkhead upstream of the IGV Figure 10. Flow distortions were then measured in the duct and at the IGV inlet plane.

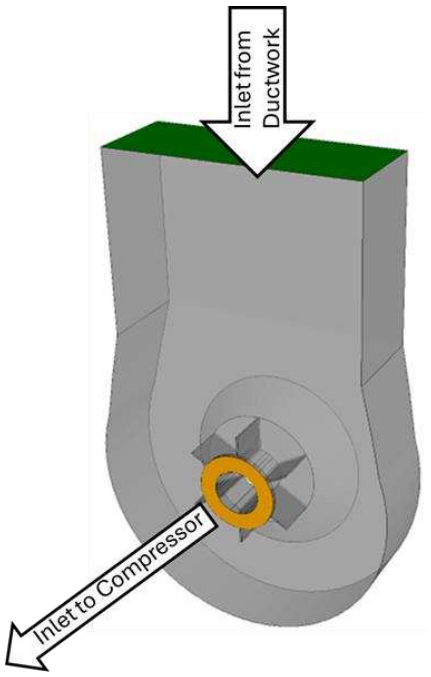

Figure 10: Air Inlet (Green) Bulkhead from Duct outlet plane to IGV Annuls Inlet Plane (Orange)

2.3 Converge CFD parameters

These cases were run with Converge CFD version 3.1. A steady solver was used to ensure that the case converged. The steady state solver monitored density at a tolerance of 0.003 measured at the outlet plane after 40 thousand cycles. A Redlich-Kwong equation of state was chosen to ensure accurate interaction of molecules during the mixing sequence. A pressure based solver was used. A base grid of 3-centimeter cubes was set, resulting in a cell count if 217,017 cells. Adaptive mesh refinement was then applied using velocity and temperature fields to ensure accurate meshing in regions with high variation, increasing cell count where needed during the simulation. Fixed embedding was set for the bulkhead and IGV plane to increase definition in this distorted zone as depicted in Figure 11.

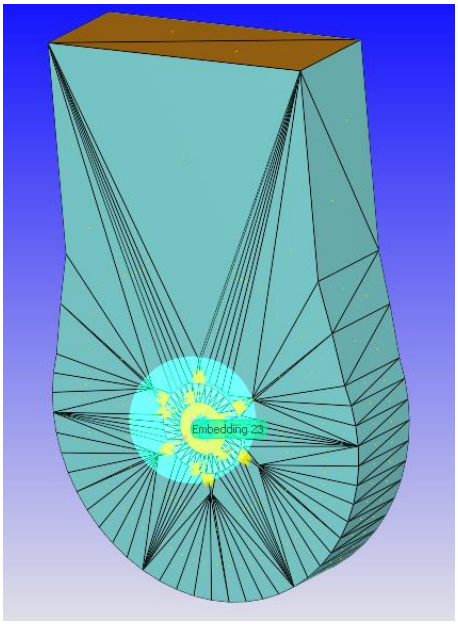

Figure 11: Bulkhead Converge Setup with Fixed Embedding 23 Shown in Teal Sphere.

A laminar vs turbulent solver study was conducted as method of minimizing computational time. Solving with laminar model provides a method of comparing cases without expending lots of computational resources. The most turbulent case, Opposed Injection 1, was modeling using both a laminar solver as well as a RANS turbulent model. The laminar case assumed no wall friction while the turbulent model had a law of wall solver. CO_2 mass fraction and velocity plots were compared to visually determine if flow patterns were similar. Variables at the inlet outlet plane and IGV plane were compared numerically to determine if the tests are numerically similar. COVs and mean value of CO_2 mass fraction, velocity, density, and mass flux were measured.

2.3.1 Boundary Conditions

Turbine inlet boundary conditions were derived from operating parameters of 1 atm, 20 ℃, and 50% actual EGR. The Centaur 40 intake flow rate 18.7 kg/s while fuel flow is approximately 0.29 kg/s at full speed and full load [12]. Table 1 outlines the defining boundary conditions defined for each zone across all simulations. It is assumed that EGR injection temperature will be ambient, a result of the cooling stage. A 50% EGR rate was selected as it represents the most challenging mixing scenario in our project scope. Exhaust composition values are listed in Table 2 at 50% EGR.

Boundary Conditions		
Zone	**Inlet Duct**	**Bulkhead**
Simulation Inlet	1 atm, 9.35 kg/s	Mapped Velocity and Mass Flow
EGR Inlet	9.35 kg/s	NA
Simulation Outlet	18.7 kg/s	100.328.64 Pa

Table 1: Boundary Conditions for Inlet Duct and Bulkhead Simulations. Each Defined Boundary Condition is Presented for Each Simulation Zone

Exhaust Gas Composition at 50% EGR	
Species	**Mass Fraction**
CO2	0.103
N2	0.769
O2	0.128

Table 2: Exhaust Gas Composition Mass Fraction at 50 Percent EGR%. Constituents calculated theoretically.

2.4 Quantification of Performance

To determine the best performing injection size, the mass flux and CO_2 mass fraction Coefficient of Variance (COV) at the outlet plane was quantified. In this study, mixing performance in the simulations was evaluated using the spatially resolved COV of CO_2 concentration in the engine intake. COVs were calculated at the outlet plane across all cells. The pressure drop was measured between the outlet plane and the EGR inlet.

The No-EGR case provided a baseline flow distortion map for the inlet duct. Total pressure distortion and mass flux distortion (MFD) was calculated using the equations 6 and 7 below. Contours of PTD, MFD and CO_2 mass fraction were plotted to visualize flow. COVs were calculated for each variable above as a method of quantifying distortion values. To determine flow effects, each parameter was then compared to the No-EGR IGV plane to determine the magnitude of distortions.

$$PTD = Total\ Pressure_{local}/Total\ Pressure_{IGV} \tag{6}$$

$$MFD = Mass\ Flux_{local}/Mass\ Flux_{IGV} \tag{7}$$

Chapter 3: Results

3.1 Laminar vs Turbulent Case Study

The Opposed Injection 1 case using a laminar solver required 99.5 core-hours on 1 cores to complete, whereas the turbulent solver required 720 core-hours on 9 cores. The laminar solver reduced computational time by 151 % total for the upper intake duct section. Although overall simulation time was comparable, the use of shared computational resources led to allocation issues.

Turbulent vs Laminar simulation results were compared numerically to determine if a laminar CFD solver will provide accurate results. Figure 12 and Figure 13 compare CO_2 mass fraction plots and velocity plots of each solver. The turbulent contours are smoother compared to the laminar cases for both CO_2 mass fraction and velocity. The collision between the two opposed jets is depicted well in both simulation cases. The well mixed stream continues down into the transition section in both models. The outlet planes exemplify similar results as well. CO_2 mass fraction planes have the same high CO_2 concentration band through the center. This same band is also observed in the velocity contour plot. While the laminar simulation model doesn't provide an exact representation of the turbulent model, the contour plots exemplify the same flow patterns throughout the duct.

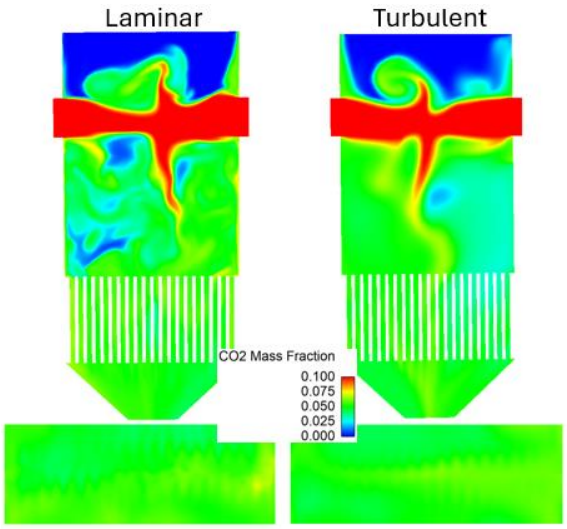

Figure 12: CO_2 Mass Fraction Contour Plots Comparing Laminar and Turbulent Simulation Models for Opposed Injection 1. Cross Section of Inlet Duct Above The Outlet Plane.

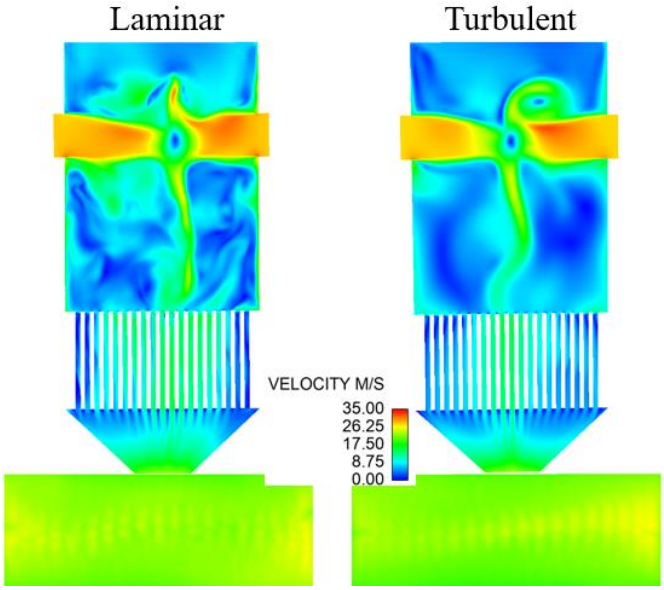

Figure 13: Velocity Contour Plots Comparing Laminar and Turbulent Simulation Models for Opposed Injection 1. Cross Section of Inlet Duct Above The Outlet Plane.

Table 3 compares the variables at the outlet plane for the laminar versus turbulent case studies. Each variable is within 1-2% of each other with CO_2 mass fraction, density and pressure all differ by less than 1 percent. Mean values are also comparable for each solver method. While laminar solver does not provide an exact replication of the turbulent solver, the values are comparable. The following cases have all been solved with a laminar flow model.

Variable	Laminar COV% (Mean Value)	Turbulent COV% (Mean Value)
CO2 Mass Fraction	10.89% (0.052)	10.56% (0.051)
Velocity (m/s)	4.58% (22.47)	5.80% (22.03)
Density (kg/m^3)	0.13% (1.21)	0.12% (1.23)
Mass Flux ($kg/m*s^2$)	4.6% (27.22)	6.05% (27.14)
Pressure (Pa)	0.019% (101323.8)	0.015% (101319.3)
Time (Core hours)	**99.5**	**720**

Table 3:Variable Comparison at Turbine Inlet Duct Outlet Plane. Coeffecicent of Variance is and Mean Value are Measued For Each Variable and Simulation Solver Model.

3.2 Turbine Inlet Duct Geometry Sweep Results

Table 4 states the simulation list as well as density COV, CO_2 mass fraction COV, and differential pressure. Figure 14 displays the relationship between CO_2 mass fraction and exhaust to EGR inlet ratio. The lesser the flow area, the higher the flow velocity, the better the mixing, and the lower the COV. This improved mixing comes at the cost of increased flow resistance, captured in Figure 15 as the relationship between pressure drop and COV. Opposed injection simulations outperform wide injection simulations for each size.

Test	Exhaust to EGR Inlet Ratio	Density CoV %	CO2 Mass Frac CoV %	Pressure Drop EGR-Outlet (Pa)
Control	1 : 1	0.83	71.77	66.78
WI1	3 : 1	0.199	15.37	513.1
WI2	2.5 : 1	0.28	20.95	363.7
WI3	2 : 1	0.42	33	263.3
WI4	1.5 : 1	0.92	71.49	144.3
WI5	1 : 1	1.06	85.44	86.7
WI6	1 : 1.5	1.11	89.67	59.4
WI7	1 : 2	1.14	91.01	40.7
OI1	3 : 1	0.13	10.89	530.6
OI2	2.5 : 1	0.18	14.39	376.1
OI3	2 : 1	0.22	17.70	261.3
OI4	1.5 : 1	0.57	49.16	137.6
OI5	1 : 1	0.67	58.72	62.1
OI6	1 : 1.5	0.78	66.94	45.6
OI7	1 : 2	0.83	67.60	39.1

Table 4: Simulation List with Results Measured at Outlet Plane.

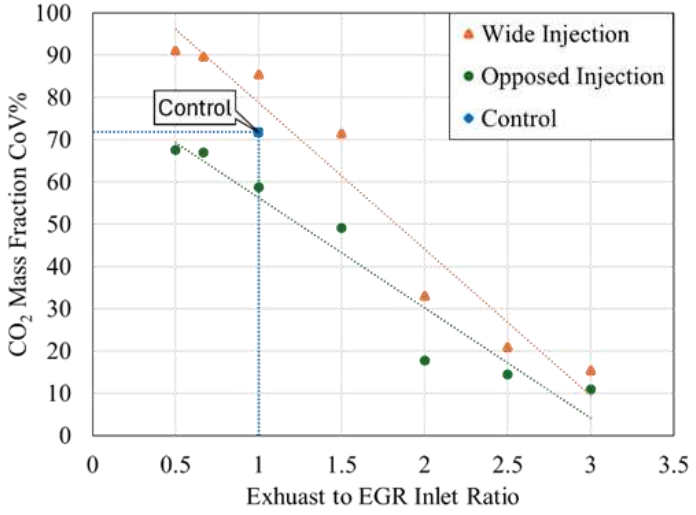

Figure 14: COV of CO_2 Mass Fraction Versus Exhaust to EGR Inlet Ratio at Outlet Plane.

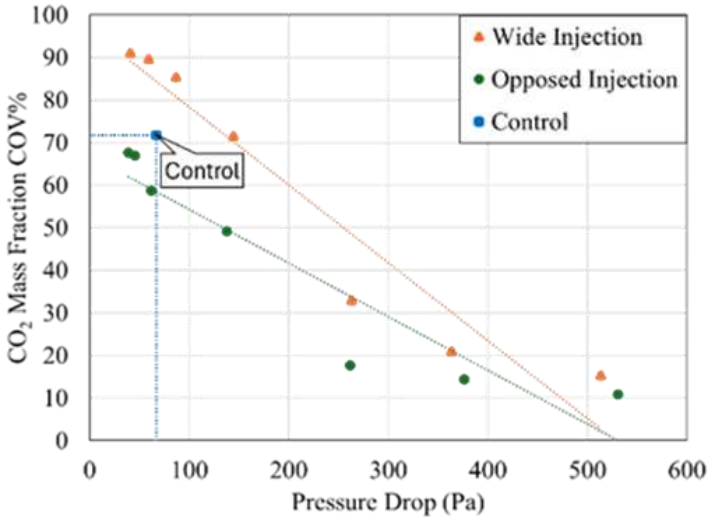

Figure 15: COV of CO_2 Mass Fraction Versus Pressure Drop At Outlet Plane.

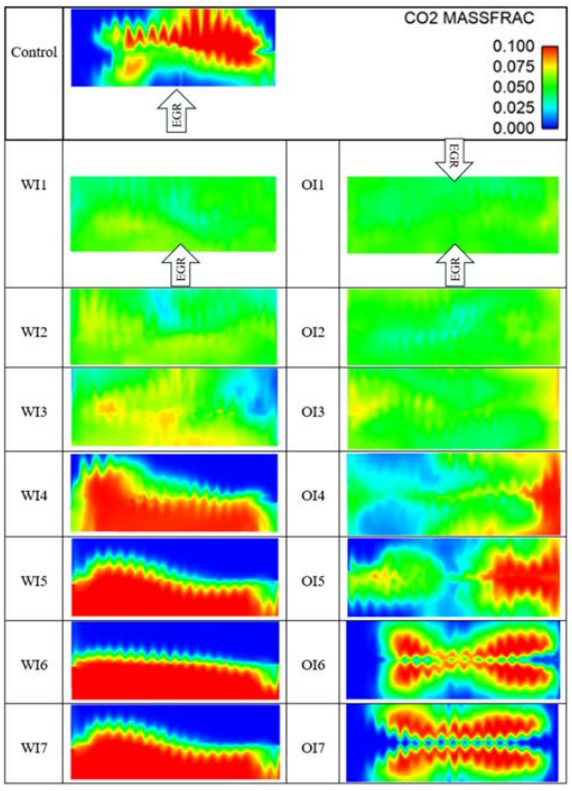

Figure 16: CO_2 Mass Fraction Contour Plots for All Cases at The Outlet Plane. EGR Arrows Show Injection Direction and Orientation.

Figure 16 shows the CO_2 mass fraction contour plots, plotted on a common scale of 0-10%. Sawtooth patterns are likely attributed to the tube style intake silencer as mentioned in §2.4. The exhaust gas from Wide-Injection (WI) cases 2-5 did not fully reach the other side of the duct, mirroring a waterfall flow, shown by a divided outlet plane which is most likely attributed to one sided injection at low pressure. The WI patterns in Figure 16 also indicate that as the EGR stream spanned the outlet plane, the COV of CO_2 mass fraction decreased as demonstrated in Figure 14. WI1, the higher-pressure and best-performing WI case, successfully reached the other side, achieving 10.9% CO_2 mass fraction COV, with the increased pressure aiding its movement across the plane.

The exhaust flow streams in the opposed injection cases collided against each other, creating a highly turbulent region. At the same area ratios, the OI cases displayed better mixing compared to WI cases for this reason. As shown in Figure 16, the distribution of CO_2 in the OI cases increased with the intensity of the flow stream impingement. The flow impingement induced turbulence is evident in the butterfly pattern in contour plots OI4 and OI5. Case OI1, which had the highest pressure and overall best performance, demonstrated a more intense impingement mixing region due to the higher pressure, contributing to its superior results, as shown in Figure 14.

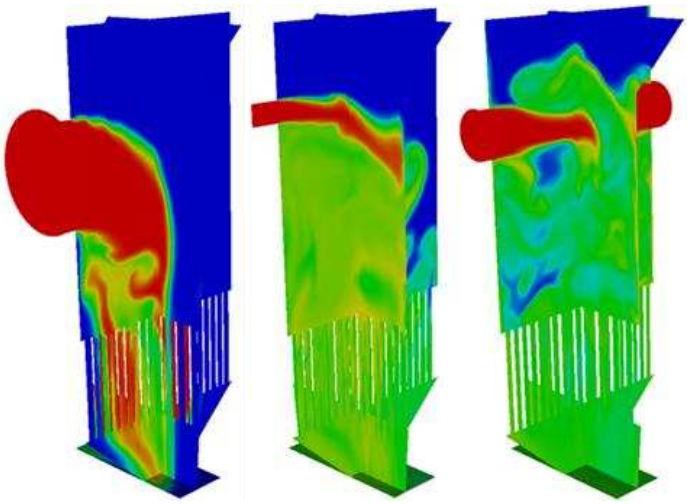

Figure 17: CO_2 Mass Fraction Contour For (Left to Right) Control, Wide Injection 1, and Opposed Injection 1 Cases.

All cases resulted in a density variation of less than 5%. Although fluid density significantly impacts blade performance, the variation is likely not substantial enough to cause issues. Figure 17 presents the relationship between density, velocity and mass flux which can be compared to the mass fraction plot. The hotspots in Figure 17 correspond to areas with a higher concentration of CO_2 which is indicative of the flow effects after the introduction of EGR. Mass flux is influenced by velocity, which is significantly altered by the higher inlet velocities associated with the high-pressure turbulence. Increased turbulence leads to better mixing but also results in larger velocity gradients. As a result, the best-mixed cases tend to have the highest velocity gradients, which as mentioned in §1.4 can cause compressor surge, potentially damaging the compressor. The best mixing case is OI1 with a mass flux COV of 4.6% as shown in Figure 17. OI1 has a pressure drop of 530.6 Pa which when combined with the application-based system pressure drop of 531.97 Pa is well under the system limit of 2488.4 Pa. It also remains within the allowable limit when combined with the surrogate system pressure drop of 916.13 Pa, for a total of 1.4 kPa.

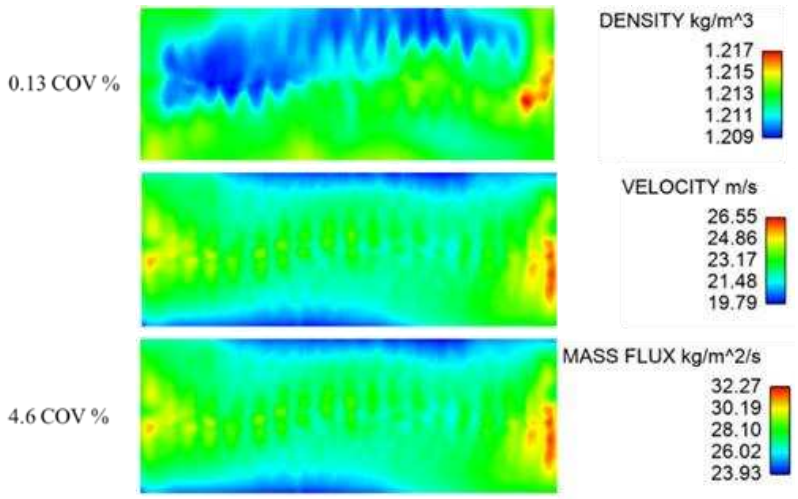

Figure 18: Density, Velocity and Mass Flux Contour Plots at the Outlet Plane of Opposed Injection.

3.3 Compressor Inlet Results

IGV plane contour plots of Normalized Mass Flux, Normalized Pressure and CO_2 Mass Fraction plotted in Figure 16. A No EGR test was performed to provide a baseline of flow distortions. The subsequent injection methods were compared against the NO EGR method and as well as the other each other. Control has lower mass flux variance and a higher pressure variance compared to the no EGR Case. Wide Injection 1 has a lower mass flux variance and higher pressure variance compared to both no EGR and control. Opposed Injection 1 has a lower variance of Mass Flux compared to no EGR, but a higher variance compared to control and Wide Injection 1. The pressure variance for opposed injection is higher than no EGR and control but less than wide injection. There is 0% CO_2 COV for the no EGR case because there is no exhaust gas injected into the intake. Control has the worst CO_2 mixing while wide injection has the best.

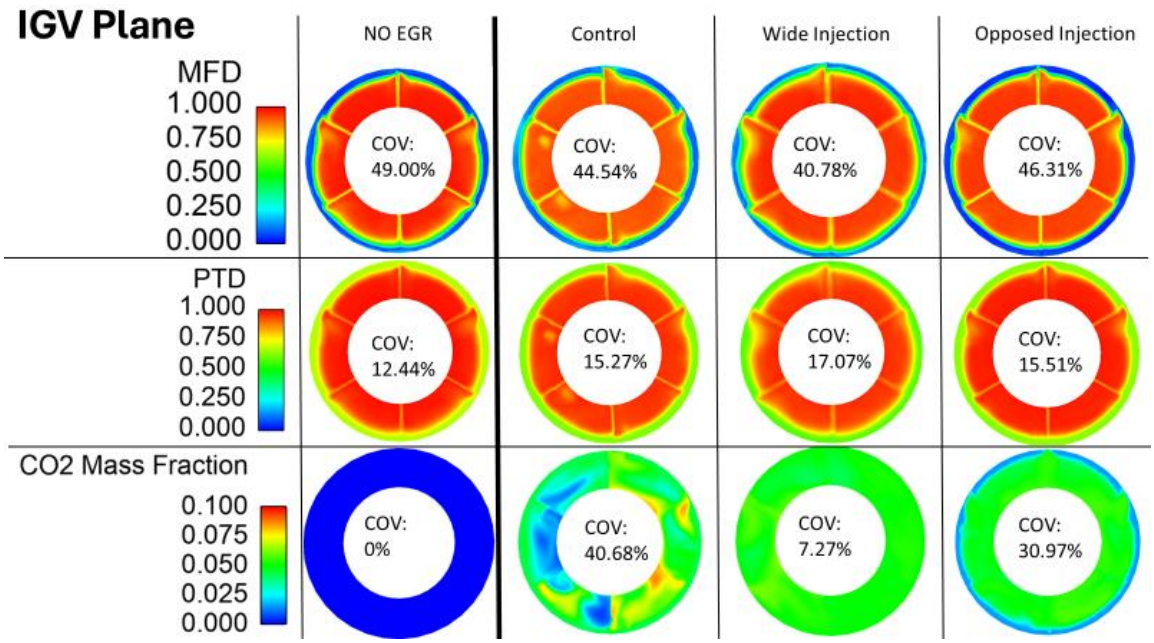

Figure 19: Mass Flux Distortion(MFD), Total Pressure Distortion (PTD) and CO_2 Mass Fraction Contours at Inlet Guide Vane (IGV) Plane.

Chapter 4: Centaur 40 Gas Turbine Commissioning

4.1 Intake and Enclosure Ductwork

Intake and enclosure ventilation ducting was mapped out and supporting flow and structure calculations were performed. Figure 20 shows the routes of each ducting system. The intake ducting weighs over 2,000 pounds and requires a robust support structure to manage the hanging weight. The main load is supported by two W4inx13 beams, while the rotating moment created by the angled jog, is counteracted with an offset turnbuckle A factor of safety of 52 was achieved for the intake structure. A maximum pressure drop of 4in-H2O constraint was met with 0.26 in-H2O. Pressure drop calculations were verified by CFD modeling. The turbine's optimal efficiency relies on a minimal intake pressure drop; a critical consideration given the engine's air intake rate of 15.3 m^3/s. Figure 21 shows the custom filter box built to integrate the gas turbine into the preexisting architecture of the building. The custom components of the intake duct were fabricated and installed in-house using 10-gauge steel.

Enclosure ventilation routes fresh air from a filter box, depicted in Figure 23, through a fan and into the package. This fresh air cools the generator and package. The generator and package exhaust are then to an outlet shown in Figure 20 and Figure 22. The enclosure duct was fabricated and installed by a local HVAC company using 22 gauge galvanized steel.

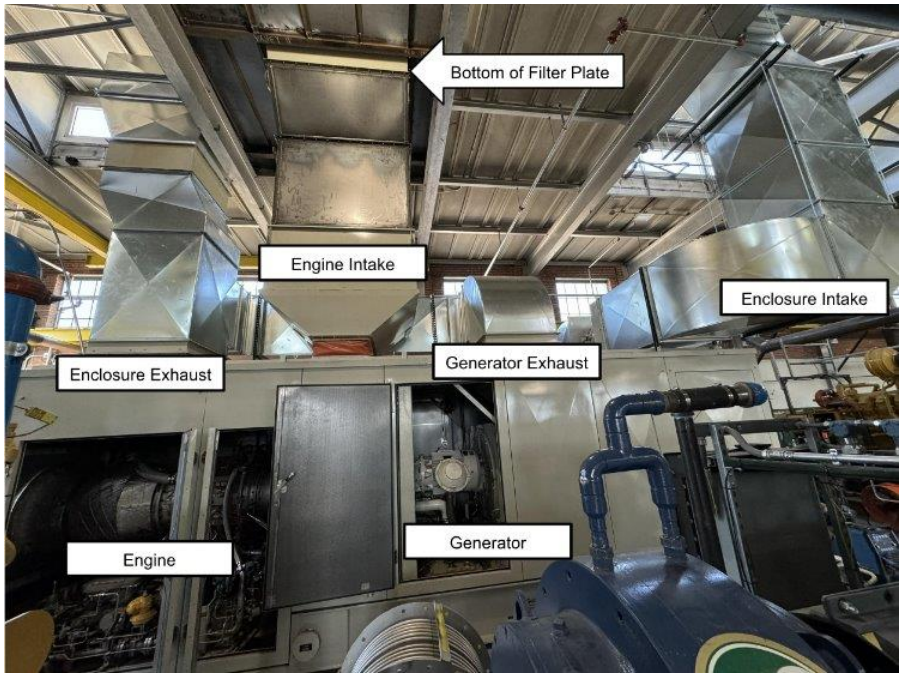

Figure 20: Ducting System Routing.

Figure 21: Custom Powerhouse Filter Box.

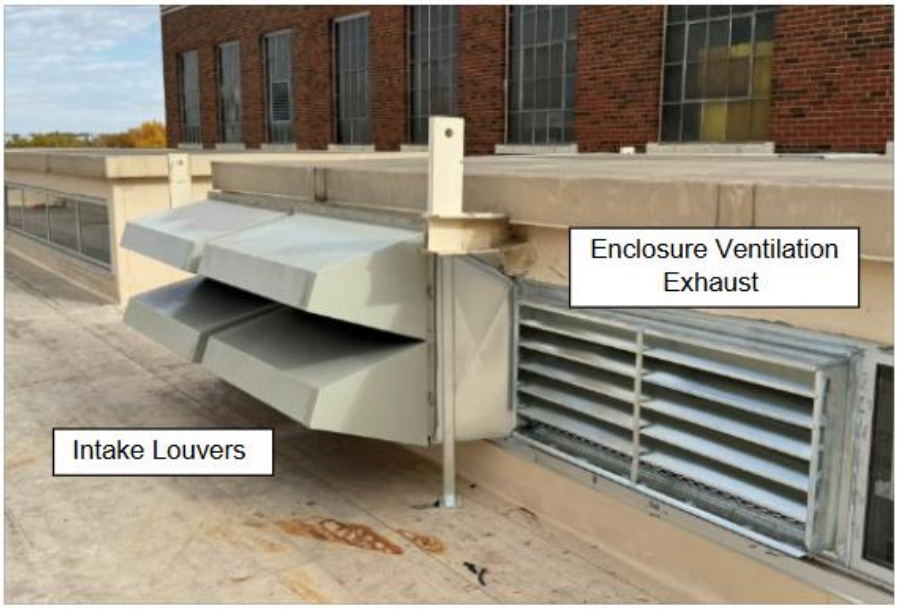

Figure 22: Intake and Enclosure Vents on Energy Powerhouse Campus Roof.

Figure 23: Enclosure Ventilation Inlet Duct.

4.2 Water Purge Supply System

This gas turbine has a compressed air purge as well as a deionized water purge. Deionized water is used to avoid contaminating the internals of the turbine engine. These two systems are used to clean out the inlet duct, compressor, and combustor from settled liquid fuels and other contaminants. Deionized water stored in tank and then pumped into the supply ports at the package inlet (Figure 24). Pump and supply pump are shown in Figure 25. The supply line is always charged to provide on demand water when the operator requires a purge procedure. A pressure diverter valve is on the pump outlet to divert the pump flow into the supply tank to avoid dead-heading the pump. Air relief valves are installed on the highpoints of the pump to bleed air out of the line during startup.

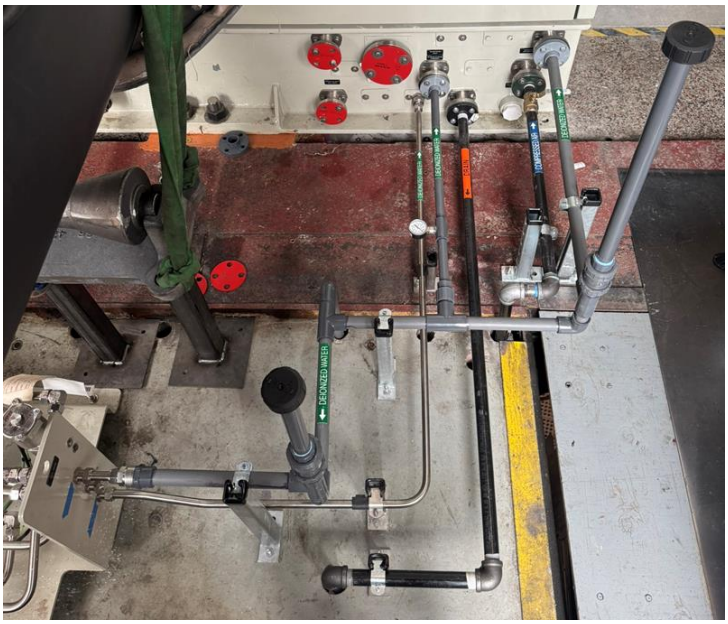

Figure 24: Water and Air Purge Supply Lines into Package.

Figure 25: Water Purge Supply Pump.

4.3 Waste System Drain

A wastewater drain system is installed as a sister system to the purge system. After the deionized water is contaminated from rinsing out the gas turbine, it is then drained into a 105 gallon wastewater tank. A liquid fuel drain is also pumped into the tank so the operator can drain the fuel lines to avoid clogging of the fuel system. A flame arrest vent is installed to prevent gaseous pressure buildup and fires. Figure 26 depicts the wastewater system.

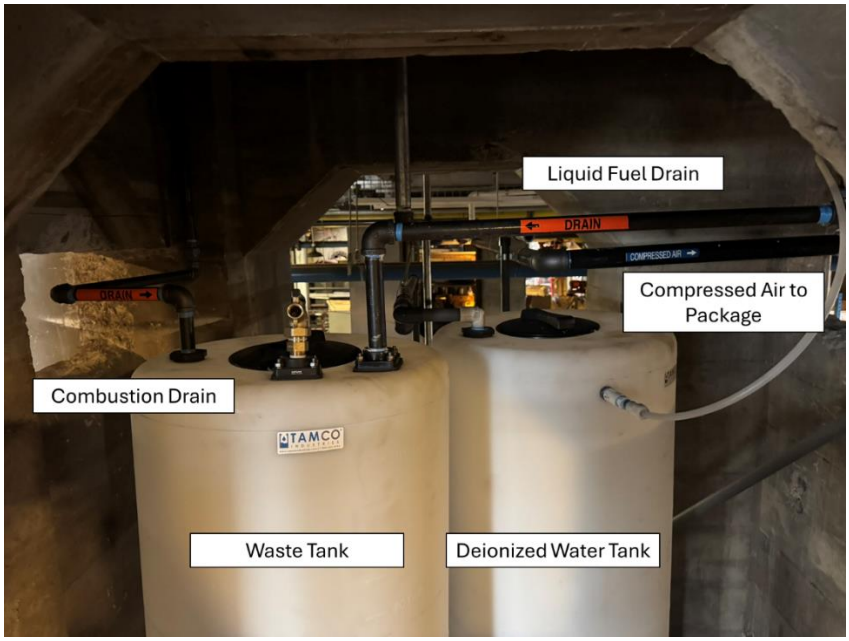

Figure 26: Wastewater Tank and Piping.

Chapter 5: Future Work and Conclusion

5.1 Conclusion

An EGR loop, coupled with a carbon capture system can effectively lower carbon emissions for a gas turbine. EGR can introduce issues that affect gas turbine performance, one of which is the mixing of exhaust gas with ambient air in the intake. Poorly mixed exhaust gas can have flow distortions that can negatively impact compressor operation. Special consideration is required to ensure that the exhaust gas mixes into the intake air to minimize flow distortions. A study was performed to investigate the design of a EGR mixer. It was found that:

- Injection method affects mass fraction distribution at IGV plane. EGR mixers were evaluated based on mixture uniformity and exhaust backpressure.
- Mixing effectiveness increase as injection inlet size decreases. This is a result of a higher velocity jets into the intake stream. Higher velocity results in a higher engine exhaust backpressure.
- Contours of CO_2 are an effective way of visualizing exhaust gas distribution.
- Contours of total pressure distortion and mass flux distortion successfully show non-uniformities in intake flow.

Control, a case simulating EGR introduction without a mixer, is the best performing case when prioritizing mass flux and pressure. Introducing EGR using a wide injection duct that was 1/3 of the exhaust cross-sectional area proved to be the optimal strategy featuring balanced mixing and minimal backpressure on the exhaust. EGR flow distortion effects were compared to a No-EGR case to determine final selection, but future work will need to be conducted to determine variation limits. A wide injection 1 mixer prototype has been designed for manufacturing, details are described in future work.

A custom filter box and duct sections were designed and built to fit the Centaur 40 into the Powerhouse Energy Institute. Flow calculations and simulations were performed to ensure the gas turbine operates at its intended design conditions before added EGR. Special consideration was made to ensure the future addition an EGR junction. The other supporting subsystems, enclosure ventilation, purge and drain were built to meet OEM specifications and conform to our lab space. A deionized water supply system provides a continuous flow of water to support purge operations. Liquid fuel drain and purge waste drain into a single 105 gallon wastewater tank. The Centaur 40 was successfully fired on August 21, 2025, and all systems functioned as expected. A testing apparatus was designed for future testing of EGR mixing performance. Six radial probes independently measure gas composition and pressure around the IGV plane as described in Future Work.

5.2 Future Work

This work provides valuable insight to the effects of EGR injection of a gas turbine inlet flow but does not provide an answer to the acceptable distortion variance. The second scope of this future work will focus on understanding the effects of inlet distortion and collecting data on gas turbine operation, with the goal of defining acceptable variance limits. This variance limit is dependent on several factors such as desired stall and surge margin as well as acceptable performance degradation. All OEMs will want to have the largest margin and the least performance loss, but every application and engine will have a different tolerance. With the Solar Turbines Centaur 40 installed at the Colorado State University's Powerhouse Energy Institute a public experimental study on inlet distortion and the effects of performance with a EGR system can be performed.

5.2.1 Mixer Construction and Install

The proposed mixer location is in the “straight section”. See Figure 30 in the appendix for a labeled intake structure. Below is a final design for the wide injection mixer. The mixer will bolt to a weld on flange using a similar flange to the existing ductwork. A weld on flange (shown in Figure 28) is required to maintain Solar Turbine’s specification of no internal hardware post filters. The mixer can be removed, and a flange cap be installed to return the engine package to a no-EGR configuration. More construction details are provided in the appendix.

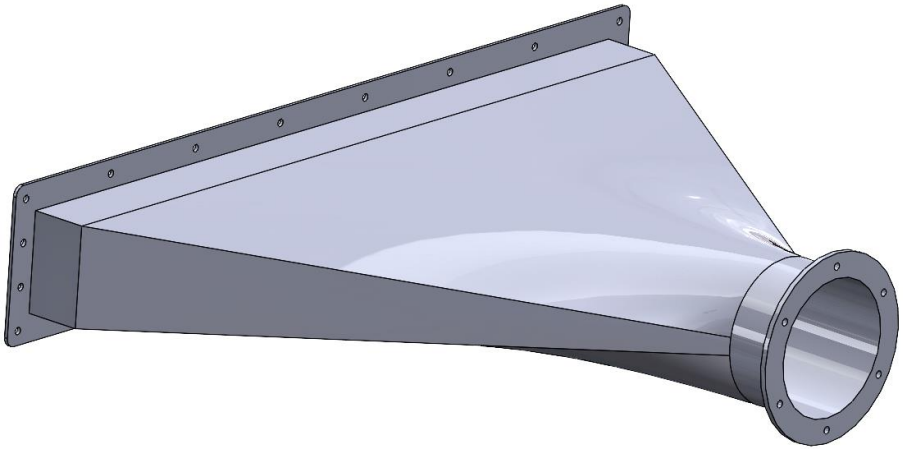

Figure 27: Wide Injection 1 Mixer Prototyped Model.

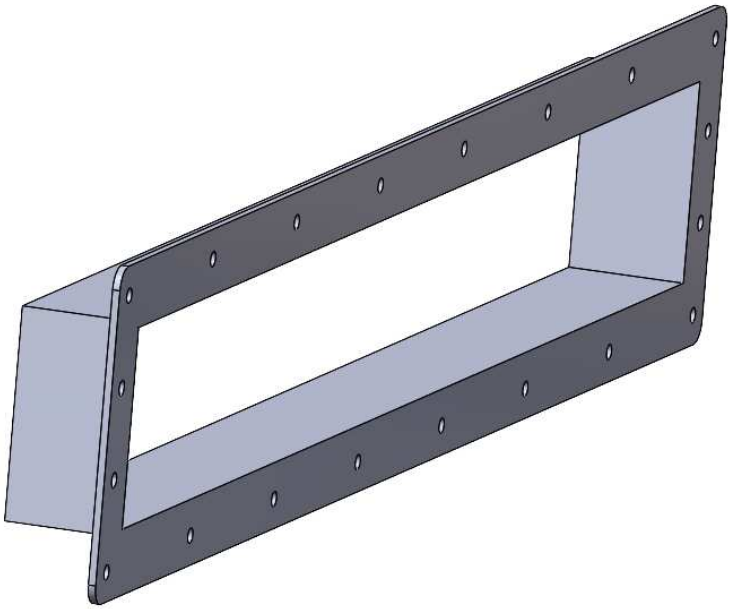

Figure 28: Weld-On Flange Adapter.

5.2.2 Experimental Test Apparatus

In order validate these simulations, a testing apparatus has been designed to collect experimental data to investigate inlet distortions and their effect on gas turbine performance. Six different sampling probes are stationed at six equally spaced locations around the IGV plane. Isolation valves allows data from each probe to be recorded separately from one another. The probe manifold outlet will have an in-line pressure transducer and fitting for connecting to a five-gas analyzer. Pressure and gas composition must be measured independently to eliminate interference from pressure effects introduced by the five-gas analyzer. Different length sampling probes can be installed to gain more radial data points. The No-EGR case will be validated prior to the mixer case to ensure model accuracy.

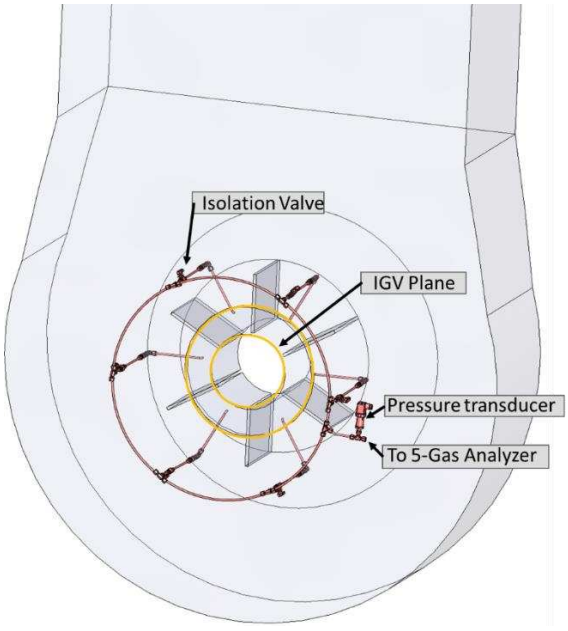

Figure 29: IGV Plane Testing Apparatus to Measure Deviations in Pressure and Gas Composition.

References

[1] "U.S. Energy Information Administration," 2024. [Online]. Available: https://www.eia.gov/totalenergy/data/browser/index.php?tbl=T11.06#/?f=A&start=2021&end=2024&charted=0-1-6. [Accessed July 2025].

[2] M. Francis, "U.S. Energy Information Administration," 9th June 2025. [Online]. Available: https://www.eia.gov/todayinenergy/detail.php?id=65445.

[3] P. S. P. D. Dan Burnes, "Study of Using Exhaust Gas Recirculation on a Gas Turbine for Carbon Capture," in *ASME Turbo Expo*, 2020.

[4] M. A. K. J. H. L. M. D. B. I. M. P. Abdul Aziz A. Aliyua, "nvestigation into simulating selective exhaust gas recirculation and varying pressurized hot water temperature on the performance of the Pilot-scale advanced CO2 capture plant with 40 wt(%) MEA," *Greenhouse Gas Control,* 2021.

[5] C. A. H. S.L. Dixon, "Axial-Flow Compressors and Ducted Fans," in *Fluid Mechanics and Thermodynamics of Turbomachinery*, 2010, pp. 143-181.

[6] I. Day, "Stall, Surge, and 75 Years of Research," *Turbomachinery,* vol. 138, no. 1, 2015.

[7] E. M. Greitzer, "Review- Axial Compressor Stall Phenomena," *Fluids Engineering,* vol. 102, pp. 131-151, 1980.

[8] D. C. D. Rabah, "FRONT BULKHEAD UPSTREAM EFFECT ON INLET IGV COMPRESSOR FLOW OF MS5002B GAS TURBINE," in *International Symposium on Heat Transfer in Gas Turbine Systems*, 2009.

[9] S. L. V. M. A. S. D. G. Ravindra Devi, "CFD Model and Design For gas Turbine Inlet Plenum With EGR," in *ASME Turbo Expo*, Boston, 2323.

[10] L. L. S. T. S. B. J. Lockyer, "Turbine Exhuast Gas Recirculation Mixer Box". US Patent 11859544, 2 January 2024.

[11] M. cave, Interviewee, *Group Manager for Compressor Aerodynamics at Solar Turbines.* [Interview]. 18 June 2025.

[12] "Centaur 40," Solar Turbines, [Online]. Available: https://www.solarturbines.com/en_US/products/power-generation-packages/centaur-40.html. [Accessed 12 2024].

[13] A. C. Dan Burnes, "Impact of Fuel Composition on Gas Turbine Engine Performance," *Engineering For Gas Turbines and Power,* 2019.

[14] T. S. D. o. M. C.-S. A. Z. M. M. Joe Hachem, "Exhaust gas recirculation applied to single-shaft gas turbines: An energy and exergy approach," *Energy,* vol. 238, 2021.

[15] E. I. K. N. S. T. K. T. K. Saitoh, "Development of combustor with exhaust gas recirculation system for the next generation gas turbine," in *Power Engineering*, Kobe, Japan, 2009.

[16] Q. X. H. Z. F. Y. X. P. J. W. Y. Liu, "Effects of CO2 and N2 Dilution on the Combustion Characteristics of H2/CO Mixture in a Turbulent, Partially Premixed Burner," *ACS Omega,* vol. 6, no. 24, pp. 15651-15662, 2021.

[17] K. H. H. T. a. D. B. R. Tao, "Response to the comments: Fuel efficiency of internal combustion engines," *Energy and Fuels,* vol. 23, no. 6, pp. 339-3342, 2009.

[18] J. E. H. a. P. E. Rokke, "Exhaust Gas Recirculation in Gas Turbines for Reduction of CO2 Emissions; Combustion Testing with Focus on Stability and Emissions," *International Journal of Thermodynamics,* vol. 8, no. 4, pp. 167-173, 2005.

[19] V. Prakash, *Parametric Emission Prediction Model in Gas Turbines with Exhaust Gas Recirculation,* Delft University of Technology, 2017.

[20] P. Bedar, "Exhaust Gas Recirculation (EGR) – Effective way to reduce NOx emissions," *Mechanical Engineering and Biomechanics,* vol. 1, no. 2, pp. 69-73, 2016.

[21] M. K. W.A. Majewski, "1.51 Emissions," in *Diesel Emissions and their Control*, SAE International, 2006.

Appendix

Intake

The intake stack is displayed in Figure 30. Air enters through the filter plate and moves downward through each duct section. The angled and straight duct sections were fabricated in house. 10 gauge steel is required by Solar Turbines to reduce vibrations. 3/8- 2 in grade 8 hex head bolts with lock washers are used to fasten each duct section together. A single-use foam crush gasket is used to seal the mating surfaces. All other holes are sealed with duct sealant compound which is applied with a putty spatula.

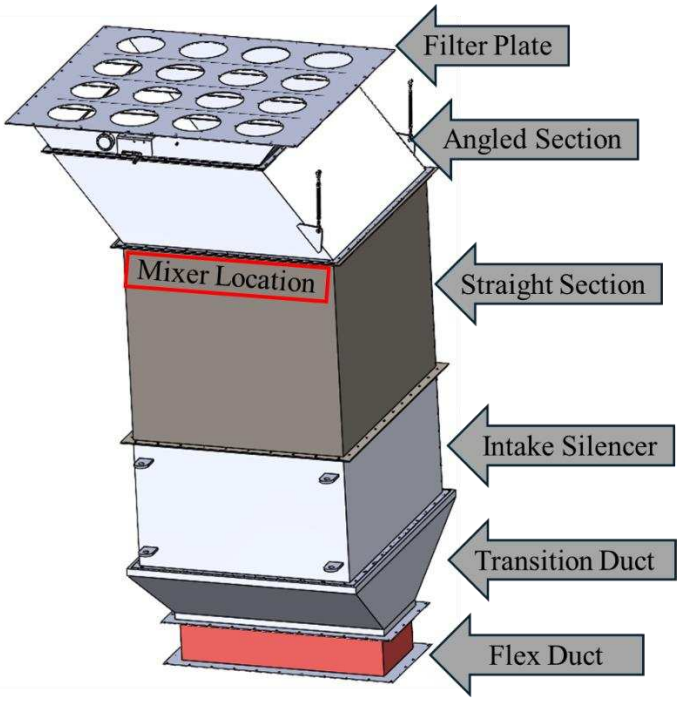

Figure 30: Intake Stack with labeled Components and Mixer Install Location in Red.

The intake stack weighs around 2,000 pounds. The supported structure is shown in Figure 31 and colored in red. The main load is supported by 2 W4inx13 beams at 12 foot long. The rotating moment is counteracted with an offset turnbuckle. The transparent red sheet is the floor

of the filter box, which seals the duct and allows for filter maintenance. 2 inch angle iron supports the floor. A point load was assumed on each beam to provide an added layer of safety. It is also assumed that the load will be equally distributed across both beams. At a 1000 pound point load the beam deflects 0.18 inches. A factor of safety of 52 for beam failure was achieved for the intake structure. The west side beams were shimmed to account for the slope of the roof.

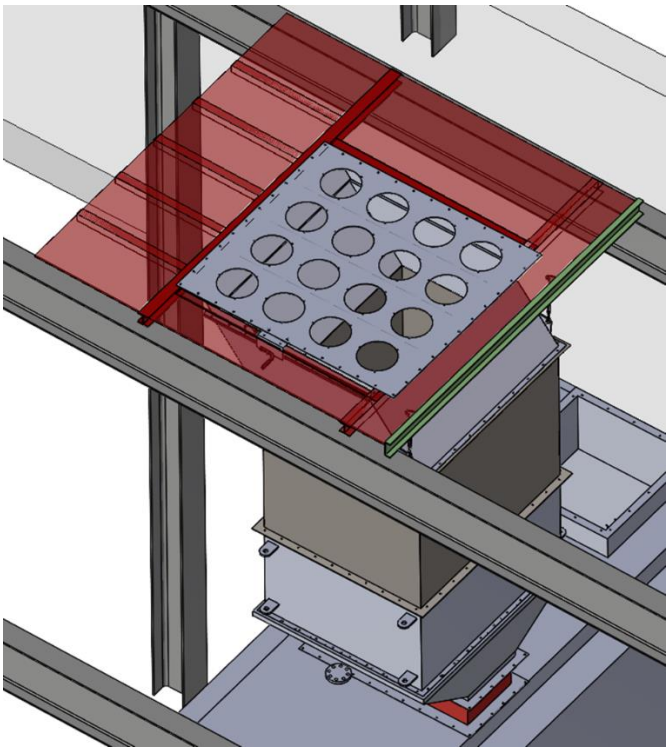

Figure 31: Intake Support Structure, Colored in Red.

Enclosure Ventilation

The enclosure HVAC ducting was designed and constructed by Hooley Heating and Air of Fort Collins. They are willing to make warranty repairs (water leaks, seal failures, etc.) to a reasonable extent and timeline.

Purge System

The purge and water wash system are supplied from a de-ionized water system from the Hydrogen refueling station project. Evan Veach, a student on the project helped install a redirect system to fill the purge supply tank. Andrew Zdanowicz is also knowledgeable on the system. The DI water skid redirects flow with a T valve and can provide a continuous flow. There is a mechanical flow switch in the tank that shuts off the supply skid when the tank is full. Water is pumped from the tank using a DAB ESY Box VFD pump system. Figure 32 shows basic menu navigation for the pump. Flow rate can be adjusted, and pressure can be viewed at the package inlet. A 1" PVC Pressure Relief valve (HAY RPV1100UPE1) allows for easy adjustment of bypass pressure using a ½ in flathead screwdriver. The valve is installed just above the tank. To vent system during a system startup, two Georg Fischer 1in vent valves (161591104) are installed at the highest points of the system. These vent valves may leak a couple of gallons of water as system primes, which is no cause for concern, unless the problem persists for over 30 seconds after pump startup.

MENU NAME	DIRECT ACCESS KEYS	HOLD-DOWN TIME
User	MODE	On releasing the button
Monitor	SET −	2 Sec
Setpoint	MODE SET	2 Sec
Manual	SET − +	5 Sec
Installer	MODE SET −	5 Sec
Technical assistance	MODE SET +	5 Sec
Reset factory values	SET +	2 sec after switching on appliance
Reset	MODE SET − +	2 Sec

Figure 32: DAB ESY Box Menu Navigation Instruction.

Wastewater System

The wastewater collection tank collects fuel contaminated water from fuel system purges. The tank should hold approximately 14 purge cycles. Tank level is to be observed manually by eye. It is extremely important not to overflow tanks, as the extra liquid will stay in package fuel piping or cause the tank to leak. When tank is full, there is a 12 foot hose attached to a ball valve to allow for drainage into disposable barrels. A 55 gallon HDPE drum is recommended for transport and disposal of the waste.

Mixer Construction

It is recommended to refer to Solar specifications to guide any unknowns. For example, flange dimensions, bolt sizing, gasket material etc. The flange dimensions and spacing were sketched for artistic purposed only, it is advised to check surrogate system flange requirements before manufacturing. The mixer will be made of 10 gauge steel to align to solar intake duct specifications. To support the cantilevered mixer, I advise using a ½ in steel cable with crimped eyes for consideration of vibrations during operation. Pipe to mixer transition length (Figure 27) is dependent on manufacturing capabilities of selected contractor. It is advised to provide an acceptable range, verified by gas distribution from a CFD simulation.

Luke at Elevation Fabrication (elevationfabrication@aol.com) has confirmed that their team can manufacture the mixer. He is knowledgeable and confident on the process, and familiar with the design. Contact when ready with finalized design.